

# Effects of prefreezing on the drying characteristics, structural formation and mechanical properties of microwave-vacuum dried apple

journal or publication title	Journal of Food Engineering
volume	244
page range	170-177
year	2019-03
URL	<a href="http://id.nii.ac.jp/1578/00002771/">http://id.nii.ac.jp/1578/00002771/</a>

doi: 10.1016/j.jfoodeng.2018.09.026

1 **Effects of Prefreezing on the Drying Characteristics, Structural Formation and**

2 **Mechanical Properties of Microwave-vacuum Dried Apple**

3  
4 Yasumasa ANDO <sup>a,\*</sup>, Shoji HAGIWARA <sup>b</sup>, Hiroshi NABETANI <sup>b,c</sup>, Itaru SOTOME <sup>c</sup>,

5 Tomoya OKUNISHI <sup>b</sup>, Hiroshi OKADOME <sup>b</sup>, Takahiro ORIKASA <sup>d,e</sup>, Akio TAGAWA <sup>f</sup>

6 <sup>a</sup> *Institute of Vegetable and Floriculture Science, NARO, 360 Kusawa, Anou, Tsu, Mie*  
7 *514-2392, Japan.*

8 <sup>b</sup> *Food Research Institute, NARO, 2-1-12 Kannondai, Tsukuba, Ibaraki 305-8642,*  
9 *Japan.*

10 <sup>c</sup> *Graduate School of Agricultural and Life Sciences, The University of Tokyo, 1-1-1*  
11 *Yayoi, Bunkyo-ku, Tokyo 113-8657, Japan.*

12 <sup>d</sup> *Faculty of Agriculture, Iwate University, 3-18-8 Ueda, Morioka, Iwate 020-8550,*  
13 *Japan.*

14 <sup>e</sup> *Agri-Innovation Center, Iwate University, 3-18-8 Ueda, Morioka, Iwate 020-8550,*  
15 *Japan.*

16 <sup>f</sup> *Professor Emeritus, Graduate School of Horticulture, Chiba University, 648 Matsudo,*  
17 *Matsudo, Chiba 271-8510, Japan.*

18  
19 Corresponding author: Yasumasa Ando, *Institute of Vegetable and Floriculture Science,*  
20 *NARO, 360 Kusawa, Anou, Tsu, Mie 514-2392, Japan.*

21 E-mail [yaando@affrc.go.jp](mailto:yaando@affrc.go.jp)

22 Tel +81-50-3533-4628

23 **Abstract**

24           The effects of prefreezing on the drying rate, internal structure and mechanical  
25 properties of apple fruit processed by microwave-vacuum drying (MVD) were  
26 evaluated. The drying rate of the prefrozen sample was approximately 1.2 to 1.3 times  
27 higher than that of the nontreated sample. In the frozen-thawed tissue, damage to the  
28 cell wall structure and cell membrane due to ice crystal formation during freezing was  
29 confirmed; thus, improvement in the drying rate was suggested to be the result of  
30 accelerated water transfer in the tissue. Structural observation using X-ray computed  
31 tomography showed that the prefrozen MVD sample had a porous internal structure  
32 with larger voids than air dried or nonpretreated samples. Alterations in the mechanical  
33 properties, such as higher maximum stress and number of peaks during the puncture  
34 test, indicating a softer and crisper texture, were observed in the prefrozen MVD  
35 sample.

36

37 **Keywords:** Microwave-vacuum drying, Prefreezing, Apple, Drying rate, X-ray CT,  
38 Mechanical property

39 **Nomenclature**

40

41	$C_m$	capacitance of cell membrane (F)
42	$E$	elastic modulus (Pa)
43	$j$	imaginary unit (–)
44	$k$	drying rate constant ( $\text{h}^{-1}$ )
45	$M$	moisture content (–)
46	$M_e$	equilibrium moisture content (–)
47	$M_0$	initial moisture content (–)
48	$P$	constant phase element exponent (–)
49	$R_i$	intracellular fluid resistance ( $\Omega$ )
50	$R_e$	extracellular fluid resistance ( $\Omega$ )
51	$R^2$	determination coefficient (–)
52	$t$	drying time (h)
53	$T$	constant phase element coefficient ( $\text{F}\cdot\text{s}^{(P-1)}$ )
54	$Z$	complex impedance ( $\Omega$ )
55	$Z_b$	combined impedance of the model (b) ( $\Omega$ )
56	$Z_{\text{CPE}}$	impedance of constant phase element ( $\Omega$ )
57	$\theta$	phase angle (rad)
58	$\sigma$	stress (Pa)
59	$\sigma_{\text{max}}$	maximum stress (Pa)
60	$\omega$	angular frequency ( $\text{rad}\cdot\text{s}^{-1}$ )

61

## 62 **1. Introduction**

63

64 Drying is one of the most classical processing methods for fruit and vegetables,  
65 resulting in an extended shelf-life, lighter weight for transportation, and reduced space  
66 requirements for storage (Dandamrongrak et al., 2002). Although dried fruit and  
67 vegetables have been commonly manufactured by relatively simple drying methods  
68 such as sun drying and air drying, newer drying techniques have been developed to  
69 reduce the drying time, as well as to improve the energy efficiency and quality of dried  
70 fruit and vegetables (Sagar and Suresh, 2010).

71 Microwave-vacuum drying (MVD) is a relatively newly developed drying  
72 technique in which water evaporation progresses rapidly because of the rapid heating of  
73 the food material, caused by the action of the microwave energy absorbed by the  
74 material in a high-frequency electric field on the water molecules in the material, and  
75 the low boiling temperature of water in the reduced-pressure environment. Application  
76 of MVD to fruit and vegetables such as cranberry (Zielinska et al., 2017a; Zielinska et  
77 al., 2017b; Yongsawatdigul and Gunasekaran, 1996), blueberry (Zielinska and  
78 Markowski, 2016; Zielinska and Michalska, 2016; Zielinska et al., 2015), banana (Jiang  
79 et al., 2014; Drouzas and Schubert, 1996), potato (Bondaruk et al., 2007), durian (Bai-  
80 Ngew et al., 2011), tomato (Orikasa et al., 2018; Abano et al., 2012; Durance and Wang,  
81 2002), mango (Pu and Sun, 2014), carrot (Nahimana and Zhang, 2011; Stępień, 2008;  
82 Cui et al., 2004; Lin et al., 1998) and apple (Chong et al., 2014; Huang et al., 2012) has  
83 been studied. It was shown that MVD has a higher drying rate (Zielinska et al., 2016;  
84 Giri and Prasad, 2007; Bondaruk et al., 2007; Durance et al., 2002; Lin et al., 1998) and

85 consumes less energy (Jiang, et al., 2017; Durance et al., 2002) than conventional air  
86 drying. Moreover, the porous structure of the dried materials allows for a high  
87 rehydration rate (Therdthai and Zhou, 2009; Giri et al., 2007; Durance et al., 2002; Lin  
88 et al., 1998) and has a different texture (Zielinska, et al., 2016; Bondaruk et al., 2007)  
89 compared to materials dried by other methods. There is also less deterioration of  
90 constituents such as ascorbic acid (Hu et al., 2006; Lin et al., 1998), carotenoids (Cui et  
91 al., 2004), chlorophyll (Hu et al., 2006; Yanyang et al., 2004; Cui, et al., 2004) owing to  
92 the prevention of excessive increases in temperature and oxidation due to the presence  
93 of air.

94           In some studies related to the drying of fruit and vegetables, the effect of  
95 pretreatment on the drying rate has been reported. It has been shown that  
96 freezing/thawing pretreatment, in particular, can effectively increase the drying rate  
97 (Dandamrongrak et al., 2002; Eshtiaghi et al., 1994). The increase in drying rate has  
98 been attributed to changes in the permeability of the cell membrane and damage of the  
99 cell wall structure of the sample tissue during freezing (Ando et al., 2016; Nieto et al.,  
100 1998; Alvarez et al., 1995). Zielinska et al. (2015) examined the effect of  
101 freezing/thawing pretreatment in the MVD of blueberries, and reported that the  
102 application of prefreezing could effectively reduce the drying time and the associated  
103 specific energy consumption.

104           The objectives of this study were to investigate the effects of the prefreezing on  
105 the MVD characteristics and post-drying structural and mechanical properties of the  
106 apple fruit, which is a popular material consumed as a dried product, and to compare the

107 quality attributes to the conventional hot-air dried sample to clarify the effectiveness of  
108 the prefreezing-MVD combination.

109

## 110 **2. Materials and methods**

111

### 112 *2.1 Sample preparation*

113 Apples (*Malus pumila* var. *domestica* cv. Fuji) were obtained from a local  
114 market and stored in a refrigerator at 5 °C prior to the experiments (within one week).  
115 The initial moisture content of the samples was gravimetrically determined according to  
116 the standard method (The Council for Science and Technology, MEXT, Japan, 2005).  
117 Briefly, the fresh sample was milled and mixed with a drying aid (Celite No.503; Imerys  
118 Filtration Minerals Inc., San Jose, USA). The aluminum cup containing the mixture was  
119 placed on a hot water bath controlled at 70 °C to predry the mixture, then the mixture  
120 was completely dried in a vacuum chamber (3606; Labline Instruments Inc., Melrose  
121 Park, USA) at a set temperature of 70 °C for 5 h. The initial moisture content of the  
122 fresh samples was  $5.377\pm 0.017$  and  $5.387\pm 0.022$  on a dry basis (g-water/g-dry) for 2  
123 lots obtained on different days, from an average of 8 samples for each lot.

124 Apples were peeled and cut into a quarter-circle shape with 10 mm thickness  
125 and 30 mm radius. The sample temperature was conditioned in an incubator (CN-25C;  
126 Mitsubishi Electric Engineering Ltd., Tokyo, Japan) at 25 °C for 1 h before drying. The  
127 sample was frozen in a freezer (HRF-90XT; Hoshizaki Corp., Aichi, Japan) at -20 °C,  
128 and stored for 6 days to 2 weeks until use for the experiment. The frozen sample was

129 thawed in the incubator at 25 °C for 3 h and used as the prefrozen-thawed sample. It  
130 was confirmed that the temperature of both nontreated and prefrozen-thawed samples  
131 reached approximately 25 °C before drying.

132

## 133 2.2 *Drying procedure and calculation of drying rate*

134 Figure 1 shows the configuration of the apparatus for MVD. In the MVD  
135 experiment, a glass desiccator was placed in a microwave oven (MOH-3000; Micro  
136 Denshi, Saitama, Japan), and the inside of the desiccator was depressurized using a  
137 vacuum pump (G-50DA; Ulvac Kiko Inc., Kanagawa, Japan). The actual microwave  
138 power output of the oven was measured by following the method of Japanese Industrial  
139 Standard (JIS) C9250: 2007 at the maximum power of 3 kW and was determined to be  
140 2.58 kW. The evaporated moisture during sample drying was collected using a cold trap  
141 (CA301; Yamato Scientific Co., Ltd., Tokyo, Japan). The pressure in the desiccator was  
142 maintained at 1.5 kPa during drying using a pressure regulation unit (NVC-2300B;  
143 EYELA, Tokyo, Japan). Eight apple samples ( $55.03 \pm 6.03$  g-fresh weight) were placed  
144 in the desiccator, and the output power of the microwave at 2450 MHz (frequency at  
145 which most commercial microwave operates) was controlled at 200, 300 or 400 W  
146 (3.63, 5.45, 7.27 W/g-fresh weight). The microwave was intermittently irradiated at a  
147 cycle of 1 min irradiation and 1 min pause to prevent the excess increase of sample  
148 temperature. The central temperature of the sample during MVD was measured using a  
149 fiber optic thermometer (FL-2000; Anritsu Meter Co., Ltd., Tokyo, Japan) with a fiber  
150 probe.



151 For air drying (AD), samples were placed in a drying chamber (DN-42; Yamato  
152 Scientific Co., Ltd.) at a controlled temperature of 40, 60 and 80 °C. The air velocity in  
153 the chamber was  $1.5 \pm 0.1 \text{ m}\cdot\text{s}^{-1}$  on average during continuous measurement over 3  
154 min. The central temperature of the sample during AD was measured using a T-type  
155 thermocouple with a wire diameter of 0.34 mm.

156 After specified drying times, the samples were removed from the drying  
157 apparatus and weighed. The moisture content was calculated from both the initial  
158 moisture content and the mass. The samples were dried until the moisture content  
159 reached below 0.2 g-water/g-dry. Based on this period, the drying rate of the samples  
160 was estimated using the exponential model which stands for the first-order reaction,  
161 incorporating a single drying rate constant for the combined effect of the various  
162 transport phenomena (Babalís et al., 2006; Orikasa et al., 2008): (1)

163 
$$\frac{M-M_e}{M_0-M_e} = \exp(-kt) ,$$

164 where  $M$ ,  $M_e$  and  $M_0$  denote the moisture content, the equilibrium moisture content and  
165 the initial moisture content respectively,  $k$  denotes the drying rate constant ( $\text{h}^{-1}$ ) and  $t$   
166 denotes the drying time (h). In this study, the constants  $k$  and  $M_e$  were estimated by  
167 using the method of least squares. After each drying, samples were dried in a  
168 thermostatic chamber at 60 °C for 12 h to remove any residual moisture and equalize  
169 the moisture condition before the evaluation of dried sample explained below.

170

### 171 2.3 *Evaluation of cell membrane damage in the sample tissue*

172 The cell membrane within the plant tissue controls the migration of moisture

173 into cells, and structural damage affects the moisture migration rate during drying  
174 processing (Vaccarezza et al., 1974). In the present study, therefore, structural damage  
175 of the cell membrane of the prefrozen sample tissue was evaluated by electrical  
176 impedance spectroscopy, which has been widely used to estimate the physiological  
177 status of various biological tissues (Zhang and Willison, 1992a, 1992b; Ando et al.,  
178 2014; Imaizumi et al., 2015; Watanabe et al., 2017).

179 Stainless steel needle electrodes spaced 10 mm apart were inserted into the  
180 sample tissue to a depth of 5 mm, then the impedance magnitude  $|Z|$  ( $\Omega$ ) and phase  
181 difference  $\theta$  (rad) of the samples before and after freeze-thawing at a frequency range  
182 from 50 Hz to 500 kHz were measured using an impedance analyzer (E4990A;  
183 Keysight Technologies, Santa Rosa, USA). The measurements were replicated 15–16  
184 times for each sample. The test was carried out at a room temperature of 25 °C.

185 The measured data were analyzed with an equivalent circuit model of cellular  
186 tissue shown in Fig. 2. Figure 2a shows a biological cell model that takes into account  
187 the capacitance of the cell membrane,  $C_m$ , and resistances of intra- and extra-cellular  
188 fluids,  $R_i$  and  $R_e$ . The model (b) shown in Fig. 2b is modified by substituting a constant  
189 phase element (CPE) for  $C_m$  in model (a) to fit the impedance characteristics of the  
190 biological tissue consisting of electrically inhomogeneous multiple cells, which  
191 produces a time constant distribution. The impedance of CPE ( $Z_{CPE}$ ) is shown as:

192 
$$Z_{CPE} = \frac{1}{(j\omega)^P T}, \quad (2)$$

193 where  $\omega$  denotes the angular frequency ( $\text{rad}\cdot\text{s}^{-1}$ ),  $T$  denotes the CPE coefficient and  $P$   
194 denotes the CPE exponent ( $0 \leq P \leq 1$ ). The combined impedance of the model (b) is

195 represented by the following equation:

$$196 \quad Z_b = \frac{R_e(Z_{CPE} + R_i)}{R_e + Z_{CPE} + R_i} .$$

197 The measured impedance data were fitted to Eq. 3 using complex nonlinear least  
198 squares curve fitting (Macdonald, 1992) and each circuit parameter was determined.<sup>(3)</sup>

199 The determination coefficient,  $R^2$ , was calculated as follows to evaluate the goodness of  
200 fit of the model (Imaizumi et al., 2015):

$$201 \quad R^2 = 1 - \frac{\sum_i (|Z_i| - |\hat{Z}_i|)^2}{\sum_i (|Z_i| - |\bar{Z}|)^2} , \quad (4)$$

202 where  $\hat{Z}$  denotes the approximate value of  $Z$ , and  $\bar{Z}$  denotes the average value of  $Z$ .

203 Here, CPE constant  $T$  was converted to apparent capacitance  $C$  using the equation  
204 below (Ando et al., 2014; Hsu and Mansfeld, 2001):

$$205 \quad C = T^{\frac{1}{P}} (R_e + R_i)^{\frac{1-P}{P}} . \quad (5)$$

206 In this study, apparent capacitance  $C$ , obtained from Eq. 5, was defined as the cell  
207 membrane capacitance,  $C_m$  (Ando et al., 2014). The detailed procedure of the equivalent  
208 circuit analysis was described in the literature (Ando et al., 2017).

209

#### 210 2.4 Microscopic observation of the sample tissue

211 The flesh tissue cut from the fresh and frozen samples before drying was fixed  
212 in a FAA solution (37 % formaldehyde: acetic acid: 50 % ethanol solution, 5: 5: 90 v/v)  
213 for 2 days, then dehydrated through a graded ethanol series (50, 70, 80, 90, 95 and  
214 100 %). The dehydrated samples were embedded in methacrylate resin (Technovit 7100;  
215 Heraeus Kulzer GmbH, Wehrheim, Germany), and sectioned into 4- $\mu$ m thick slices

216 using a microtome (RM2145; Leica, Wetzlar, Germany). The sections were stained with  
217 safranine (Wako, Osaka Japan) and Fast green FCF (Wako, Osaka Japan) solutions, and  
218 observed with an optical microscope (DM LB; Leica) equipped with a digital camera  
219 ( $\alpha$ 5100; Sony, Tokyo, Japan).

220

## 221 2.5 *Visualization of the internal structure of the dried sample*

222 A micro focus X-ray computed tomography (X-ray CT) system (SMX-100CT;  
223 Shimadzu Corp., Kyoto, Japan) was used for the observation of both the whole structure  
224 and microstructure of the dried samples. The dried samples were scanned using the X-  
225 ray CT system at an X-ray tube voltage of 70 kV and current of 40  $\mu$ A. For observation  
226 of the microstructure, the center part of the dried sample was cut with a sharp knife into  
227 a small block (3 mm  $\times$  3 mm  $\times$  6 mm), and scanned at a voltage of 50 kV and current of  
228 40 mA. For both observations, 1200 transmission images were obtained through 360  
229 degree rotation. The tomographic images of the dried sample were reconstructed using  
230 software (Exfact VR; Nihon Visual Science Inc., Tokyo, Japan).

231

## 232 2.6 *Mechanical properties of the dried sample*

233 A universal testing machine (5542; Instron, Norwood, USA) equipped with a  
234 500 N load cell was used for the puncture test of dried samples. The dried sample was  
235 placed on a metal base with a 10 mm diameter hole in the center, then a cylindrical  
236 plunger 3.2 mm in diameter was inserted at a speed of 1 mm $\cdot$ s<sup>-1</sup> into the center flat  
237 surface of the sample until the plunger passed through the center of the hole and

238 completely penetrated the sample. The trigger load was set to 0.05 N. The thickness at  
239 the center flat part of the sample was measured using a caliper.

240 The value of stress  $\sigma$  was calculated by dividing the measured force with the  
241 cross-sectional area of the plunger, and the strain was calculated by dividing the  
242 displacement with the thickness of the punctured part of the sample. Maximum stress  
243  $\sigma_{\max}$  (Pa), elastic modulus  $E$  (Pa), and number of peaks were calculated as indices of the  
244 mechanical properties. The value of  $E$  was defined as the slope of the first linear part of  
245 the stress-strain curve. The number of peaks refers to the number of positive peaks  
246 greater than a threshold force counted on the force-deformation curve, and has been  
247 used as one of the indices of the crispness of dry material (Dogan and Kokini, 2007).  
248 The value of the threshold was set at 0.044 N, equivalent to 15 % of the average drop  
249 off force value of all tested samples (Dogan and Kokini, 2007). The number of peaks  
250 were calculated only for the prefrozen AD and MVD samples in order to compare their  
251 crispness. The experiments were replicated 16–18 times for each sample. The test was  
252 carried out at a room temperature of 25 °C.

253

### 254 2.7 *Statistical analysis*

255 Statistical analyses were performed using R software version 3.3.3 (R Core  
256 Team (2017)).

257

## 258 **3. Results and discussion**

259

260 3.1 *Structural changes in the cell wall and cell membrane after freeze-thawing*

261 Figure 3 shows microscopic images of the apple flesh tissue before and after  
262 freeze-thawing. In the nonfrozen tissue, round shape cells 300 to 500  $\mu\text{m}$  in diameter  
263 were densely arranged and small intercellular spaces were observed (Fig. 3a). However,  
264 in the frozen-thawed sample tissue shown in Fig. 3b, the intercellular spaces were  
265 greatly expanded to the large indefinite shape spaces approximately 500 to 1000  $\mu\text{m}$  in  
266 length, and cells were markedly shrunk. This phenomenon is thought to result from the  
267 dehydration of intracellular fluid accompanied with the growth of ice crystals formed in  
268 the extracellular area. Because of this ice crystal formation process, the original cell  
269 wall structure was destroyed, leaving large spaces as previously reported by Chassagne-  
270 Berces et al. (2009).

271 The parameters of the equivalent circuit model (b) in Fig. 2, estimated from the  
272 electrical impedance characteristics, are shown in Table 1. The values of  $R^2$  in the model  
273 fitting were over 0.999 and 0.998 for nonfrozen and frozen-thawed samples,  
274 respectively, indicating that the model is suitable to describe the impedance  
275 characteristics of the samples. During a freeze-thaw cycle, cells are subjected to a  
276 multitude of stresses including chilling stress, and mechanical and chemical stresses  
277 resulting from ice crystal formation (Steponkus, 1984). It has been demonstrated that  
278 ion leakage in cell membrane occurs prior to freezing injury (Palta, 1990), suggesting  
279 that the loss of osmotic responsiveness of plant cells may be due to low-temperature-  
280 induced alterations in the plasma membrane structure (Marangoni et al., 1996). The  
281 decrease in the extracellular fluid resistance,  $R_e$ , and increase in the intracellular fluid

282 resistance,  $R_i$ , shown in Table 1 could be explained by the changes in the intra- and  
283 extracellular electrolyte concentrations, caused by the leakage of the intracellular fluid  
284 to the extracellular region resulted from the cell membrane damage during freezing-  
285 thawing process.

286 The cell membrane capacitance,  $C_m$ , decreased after freeze-thawing. The same  
287 phenomenon has been reported for potatoes (Imaizumi et al., 2015; Zhang et al., 1993)  
288 and spinach (Watanabe et al., 2017) during heating. The high  $C_m$  value of the fresh  
289 tissue is thought to be attributable to the lipid bilayer structure of the membrane  
290 (Ashrafuzzaman and Tuszynski, 2013); therefore, the decrease in  $C_m$  of the frozen-  
291 thawed sample observed in this study is suggested to be a result of the structural  
292 destruction of the cell membrane due to ice crystal formation during freezing.

293

### 294 3.2 *Effect of prefreezing on the drying rate of apple samples*

295 Figure 4a shows the changes in the moisture content versus drying time for the  
296 nontreated and prefrozen-thawed samples during AD. For both samples, the moisture  
297 content decreased faster at higher drying temperatures. Compared to the nontreated  
298 sample, the drying of prefrozen samples progressed rapidly, even at the same drying  
299 temperature. As with AD, prefrozen samples dried faster than nontreated samples during  
300 MVD (Fig. 4b). At the beginning of the MVD process, the initial moisture content of  
301 the prefrozen sample declined because the internal moisture was squeezed from the  
302 damaged tissue when the pressure was reduced to the target value of 1.5 kPa.

303 Solid and dashed lines in the figure represent the least squares regression

304 analysis of the exponential model (Eq. 1). The correlation coefficient showed a good fit  
305 with the experimental data ( $0.996 \leq R^2$ ), indicating that the model is appropriate for  
306 characterizing the changes in the moisture content of apples during drying. The drying  
307 rate constant  $k$  values estimated from the analysis are shown in Table 2. Although the  
308 values of  $k$  of MVD cannot be compared with those of AD under the same temperature  
309 condition, the values tended to be higher by roughly 3 to 4 times than those of AD. The  
310 higher drying rate in MVD was attributed to the promotion of moisture transfer from the  
311 interior of the drying sample to the surface, due to the microwave irradiation that  
312 penetrates the sample interior and selectively acts on the contained water molecules.  
313 The prefrozen sample showed approximately 1.2 to 1.3 times higher values of  $k$   
314 compared to those of nontreated samples in both AD and MVD. As mentioned  
315 previously, the cell wall structure and cell membrane were damaged by ice crystal  
316 formation during freezing. Therefore, it was proposed that the increased drying rate of  
317 prefrozen samples was due to the accelerated water permeability of the sample tissue  
318 following the structural collapse of the cell wall and membrane, as reported by Alvarez  
319 et al. (1995), who claimed that the disruption of membranes and degradation of the  
320 middle lamella and hemicellulosic polysaccharides present in the cell wall enhanced  
321 moisture diffusivity in the plant tissue during air drying. In terms of cell membranes, the  
322 previous study in which the impedance characteristics of the potato tissue was  
323 monitored during drying has revealed that the cell membranes were gradually damaged  
324 from the initial moisture content to 1.0 (dry basis) suggesting that the water  
325 permeability in the tissue increased even during drying (Ando et al., 2014). In this study,



326 however, high water permeability was maintained throughout the drying process by  
327 preliminarily destroying the cell membrane, leading to higher drying rate. Especially in  
328 MVD, the drying time required was reduced by about half at each microwave power  
329 condition due to the decreased initial moisture content, resulting from the reduced  
330 pressure treatment and increased drying rate.

331           Figure 5 shows changes in the temperature of the center part of the samples  
332 until the end of drying. In the AD sample, temperature elevations of the prefrozen  
333 samples tended to be suppressed compared to the nonfrozen samples at each drying  
334 temperature (Fig. 5a); this was because the applied heat was more efficiently utilized by  
335 the phase change (evaporation) of water at a high rate of drying in the prefrozen  
336 samples. In the MVD of nonfrozen samples, the center temperature was gradually  
337 increased to approximately 70 °C at each drying temperature, by utilizing temperature  
338 cycling in the irradiation-pause cycle of the microwave (Fig. 5b). In the MVD, the  
339 boiling point of the sample was increased even in the reduced pressure because the  
340 sample moisture was concentrated as drying proceeded. Also, the supplied microwave  
341 energy per moisture amount was increased as the moisture decreased during drying. In  
342 addition to these conditions, drying rate of the nonfrozen sample was low especially in  
343 the end of drying, therefore, temperature was not suppressed and kept increasing. The  
344 temperature of the prefrozen MVD sample decreased from initial temperature of 25 °C  
345 to about 20 °C at first 0.5 h because of the decreased boiling point in the reduced  
346 pressure environment and the efficient absorption of latent heat due to the high drying  
347 rate of the prefrozen sample. The temperature maintained below 40 °C until end of the

348 drying at each microwave power condition while the temperature of the nontreated  
349 sample was not suppressed because of the low water evaporation rate during drying.  
350 The result indicates that applied microwave energy was spend more effectively for  
351 water evaporation in the prefrozen MVD sample.

352

### 353 3.3 *Effects of prefreezing on the structural and mechanical properties of dried* 354 *samples*

355 Figure 6 shows the reconstructed images and tomograms of the dried samples.  
356 The prefrozen AD sample showed less shrinkage during drying compared to the  
357 nonfrozen AD sample. In the nonfrozen AD sample (Fig. 6a), fine internal voids were  
358 scattered throughout and a dense internal structure was observed; whereas a porous  
359 internal structure with relatively larger voids, 200–400  $\mu\text{m}$  in diameter, was observed in  
360 the prefrozen AD sample (Fig. 6b). The shrinkage of prefrozen AD sample was  
361 inhibited because the spaces formed by ice crystal formation during freezing (as shown  
362 in Fig. 3b) functioned as a vent and the pressure difference between the inside and  
363 surface of the sample tissue, which is a driving force of shrinkage during drying, was  
364 mitigated.

365 In the nonfrozen MVD sample shown in Fig. 6c, the center part appeared to be  
366 tightly compressed and formed a dense structure (white region in the image), while a  
367 porous structure is observed in the surface region. In the microstructure image, both  
368 dense and porous areas can be observed. Figure 7 shows the mechanism of the structural  
369 formation of MVD samples. In the nonfrozen sample tissue, the expanded internal water

370 vapor generated under microwave irradiation, in which heating proceeds from the center  
371 of the sample, leaked slightly from the tissue through the intercellular gaps. During the  
372 following pause in microwave irradiation, the remaining gas within the tissue is cooled  
373 and attempts to return to its original volume. However, the amount of the gas was  
374 reduced because of the leakage during irradiation, and as a result, the sample volume  
375 shrunk because the pressure within the tissue became negative. The dense structure of  
376 the MVD nonfrozen samples was attributed to the repetition of this cycle.

377           Since the cell wall and membrane structures of the frozen-thawed tissue were  
378 damaged and characterized by high gas permeability, the generated gas during  
379 microwave heating is able to pass through the tissue at a higher rate than in the  
380 nonfrozen tissue. Even during the cooling phase, a high permeability was maintained,  
381 and therefore, the tissue showed less shrinkage due to the mitigation of pressure  
382 differences between the interior and exterior. As a result, the porous structure of the  
383 prefrozen MVD sample showed void diameters of 400–600  $\mu\text{m}$  (Fig. 6d). The  
384 microwave puffing which is a rapid volume expansion of a sample at relatively low  
385 moisture content that occurs during microwave treatment (Zhen et al., 2013; Rakesh and  
386 Datta, 2011) was not observed in this study because the internal pressure required for  
387 the puffing was not generated as mentioned above, and also because the microwave  
388 power output was relatively low. The more porous structure of the prefrozen MVD  
389 sample compared to the prefrozen AD sample suggests that heating and moisture  
390 evaporation from the interior during microwave irradiation acted as a force radiating  
391 from the sample interior.

392 Typical puncture curves and mechanical parameters for the dried samples are  
393 shown in Fig. 8 and Table 3, respectively. The high value of maximum stress  $\sigma_{\max}$   
394 observed in the nonfrozen MVD samples was attributed to the densely compressed  
395 nature of the sample, as shown in Fig. 6c. The puncture curve of the nonfrozen AD  
396 sample showed a smooth shape, and the sample showed a significantly lower  $E$  value,  
397 which is used as a measure of stiffness, despite the almost identical value of  $\sigma_{\max}$  as the  
398 prefrozen AD sample. The similar shape of the puncture curves with many peaks  
399 observed in the prefrozen AD and MVD samples could originate from the porous  
400 internal structure containing many separate compartments. The prefrozen MVD sample  
401 showed a smaller  $\sigma_{\max}$  value and about twice the number of peaks compared to the  
402 prefrozen AD sample. Dogan and Kokini (2007) reported that the number of peaks was  
403 correlated with sensory crispness in an experiment using corn extrudates. Therefore, the  
404 higher number of peaks in the prefrozen MVD sample indicates that the sample is  
405 crisper than the prefrozen AD sample, and it is suggested that the softer and crisper  
406 property of the prefrozen MVD sample is due to its brittle structure with larger internal  
407 voids.

408

#### 409 **4. Conclusions**

410

411 The findings obtained from the present study, i.e., the relation of the drying rate  
412 and the cellular damage, and the mechanism of structural formation during MVD can be  
413 valuable in effectively manufacturing dried foods with a unique texture. Evaluation of

414 production energy costs and quality, such as flavor or nutrient components, and  
415 development of a recovery and recycling technique for drip discharged from the sample  
416 under reduced pressure should be addressed as future works. In addition, the suitable  
417 prefreezing conditions (e.g., temperature and time) should be investigated to maximize  
418 the drying rate and energy efficiency for industrial application.

419

#### 420 **Acknowledgement**

421

422 This study was supported by a research grant of the Society of Agricultural  
423 Structures, Japan.

424

#### 425 **References**

426

427 Abano, E. E., Ma, H., & Qu, W. (2012). Influence of combined microwave-vacuum  
428 drying on drying kinetics and quality of dried tomato slices. *Journal of Food*  
429 *Quality*, 35, 159–168.

430 Alvarez, C. A., Aguerre, R., Gómez, R., Vidales, S., Alzamora, S. M., & Gerschenson,  
431 L. N. (1995). Air dehydration of strawberries: Effects of blanching and osmotic  
432 pretreatments on the kinetics of moisture transport. *Journal of Food Engineering*,  
433 25(2), 167–178.

434 Ando, Y., Mizutani, K., & Wakatsuki, N. (2014). Electrical impedance analysis of potato  
435 tissues during drying. *Journal of Food Engineering*, 121, 24–31.

- 436 Ando, Y., Maeda, Y., Mizutani, K., Wakatsuki, N., Hagiwara, S., & Nabetani, H. (2016).  
437 Impact of blanching and freeze-thaw pretreatment on drying rate of carrot roots  
438 in relation to changes in cell membrane function and cell wall structure. *LWT -*  
439 *Food Science and Technology*, 71, 40–46.
- 440 Ando, Y., Hagiwara, S., & Nabetani, H. (2017). Thermal inactivation kinetics of pectin  
441 methylesterase and the impact of thermal treatment on the texture, electrical  
442 impedance characteristics and cell wall structure of Japanese radish (*Raphanus*  
443 *sativus* L.). *Journal of Food Engineering*, 199, 9–18.
- 444 Ashrafuzzaman, M., & Tuszynski, J. A. (2013). Structure of membranes. In *Membrane*  
445 *Biophysics* (pp.9–30). Springer-Verlag Berlin Heidelberg.
- 446 Bondaruk, J., Markowski, M., & Błaszczak, W. (2007). Effect of drying conditions on  
447 the quality of vacuum-microwave dried potato cubes. *Journal of Food*  
448 *Engineering*, 81, 306–312.
- 449 Babalis, S. J., Papanicolaou, E., Kyriakis, N., & Belessiotis, V. G. (2006). Evaluation of  
450 thin-layer drying models for describing drying kinetics of figs (*Ficus carica*).  
451 *Journal of Food Engineering*, 75(2), 205–214.
- 452 Bai-Ngew, S., Therdthai, N., & Dhamvithee, P. (2011). Characterization of microwave  
453 vacuum-dried durian chips. *Journal of Food Engineering*, 104, 114–122.
- 454 Chassagne-Berces, S., Poirier, C., Devaux, M., Fonseca, F., Lahaye, M., Pigorini, G.,  
455 Girault, C., Marin, M., & Guillon, F. (2009). Changes in texture, cellular  
456 structure and cell wall composition in apple tissue as a result of freezing. *Food*  
457 *Research International*, 42(7), 788–797.

- 458 Chong, C. H., Figiel, A., Law, C. L., & Wojdyło, A. (2014). Combined drying of apple  
459 cubes by using of heat pump, vacuum-microwave, and intermittent techniques.  
460 *Food and Bioprocess Technology*, 7, 975–989.
- 461 Cui, Z., Xu, S., & Sun, D. (2004). Microwave–vacuum drying kinetics of carrot slices.  
462 *Journal of Food Engineering*, 65, 157–164.
- 463 Cui, Z., Xu, S., & Sun, D. (2004). Effect of microwave-vacuum drying on the  
464 carotenoids retention of carrot slices and chlorophyll retention of Chinese chive  
465 leaves. *Drying Technology*, 22 (3), 563–575.
- 466 Dandamrongrak, R., Young, G., & Mason, R. (2002). Evaluation of various pre-  
467 treatments for the dehydration of banana and selection of suitable drying models.  
468 *Journal of Food Engineering*, 55(2), 139–146.
- 469 Dogan, H., & Kokini, J. L. (2007). Psychophysical markers for crispness and influence  
470 of phase behavior and structure. *Journal of Texture Studies*, 38, 324–354.
- 471 Drouzas, A. E., & Schubert, H. (1996). Microwave application in vacuum drying of  
472 fruits. *Journal of Food Engineering*, 28, 203–209.
- 473 Durance, T. D., & Wang, J. H. (2002). Energy consumption, density, and rehydration  
474 rate of vacuum microwave- and hot-air convection- dehydrated tomatoes.  
475 *Journal of Food Science*, 67 (6), 2212–2216.
- 476 Eshtiaghi, M. N., Stute, R., & Knorr, D. (1994). High-pressure and freezing  
477 pretreatment effects on drying, rehydration, texture and color of green beans,  
478 carrots and potatoes. *Journal of Food Science*, 59(6), 1168–1170.
- 479 Giri, S. K., & Prasad, S. (2007). Drying kinetics and rehydration characteristics of

480 microwave-vacuum and convective hot-air dried mushrooms. *Journal of Food*  
481 *Engineering*, 78, 512–521.

482 Hsu, C. H., & Mansfeld, F. (2001). Technical note: Concerning the conversion of the  
483 constant phase element parameter Y-0 into a capacitance. *Corrosion*, 57(9),  
484 747–748.

485 Hu, Q., Zhang, M., Mujumdar, A. S., Xiao, G., & Sun, J. (2006). Drying of edamames  
486 by hot air and vacuum microwave combination. *Journal of Food Engineering*,  
487 77, 977–982.

488 Huang, L., Zhang, M., Wang, L., Mujumdar, A. S., & Sun, D. (2012). Influence of  
489 combination drying method on composition, texture, aroma and microstructure  
490 of apple slices. *LWT - Food Science and Technology*, 47, 183–188.

491 Imaizumi, T., Tanaka, F., Hamanaka, D., Sato, Y., & Uchino, T. (2015). Effects of hot  
492 water treatment on electrical properties, cell membrane structure and texture of  
493 potato tubers. *Journal of Food Engineering*, 162, 56–62.

494 Jiang, H., Zhang, M., Mujumdar, A. S., & Lim, R. (2014). Comparison of drying  
495 characteristic and uniformity of banana cubes dried by pulse-spouted microwave  
496 vacuum drying, freeze drying and microwave freeze drying. *Journal of the*  
497 *Science of Food and Agriculture*, 94, 1827–1834.

498 Jiang, N., Liu, C., Li, D., Zhang, Z., Liu, C., Wang, D., Niu, L., & Zhang, M. (2017).  
499 Evaluation of freeze drying combined with microwave vacuum drying for  
500 functional okra snacks: Antioxidant properties, sensory quality, and energy  
501 consumption. *LWT - Food Science and Technology*, 82, 216–226.



502 Lin, T. M., Durance, D., & Scaman, C. H. (1998). Characterization of vacuum  
503 microwave, air and freeze dried carrot slices. *Food Research International*, 31  
504 (2), 111–117.

505 Macdonald, J. R. (1992). Impedance spectroscopy. *Annals of Biomedical Engineering*,  
506 20(3), 289–305.

507 Marangoni, A. G., Palma, T., & Stanley, D. W. (1996). Membrane effects in postharvest  
508 physiology. *Postharvest Biology and Technology*, 7(3), 193–217.

509 Nahimana, H., & Zhang, M. (2011). Shrinkage and color change during microwave  
510 vacuum drying of carrot. *Drying Technology*, 29, 836–847.

511 Nieto, A., Salvatori, D., Castro, M. A., & Alzamora, S. M. (1998). Air drying behaviour  
512 of apples as affected by blanching and glucose impregnation. *Journal of Food*  
513 *Engineering*, 36(1), 63–79.

514 Orikasa, T., Wu, L., Shiina, T., & Tagawa, A. (2008). Drying characteristics of kiwifruit  
515 during hot air drying. *Journal of Food Engineering*, 85(2), 303–308.

516 Orikasa, T., Koide, S., Sugawara, H., Yoshida, M., Kato, K., Matsushima, U., Okada,  
517 M., Watanabe, T., Ando, Y., Shiina, T., & Tagawa, A. (2018). Applicability of  
518 vacuum-microwave drying for tomato fruit based on evaluations of energy cost,  
519 color, functional components and sensory qualities. *Journal of Food Processing*  
520 *and Preservation*, <https://doi.org/10.1111/jfpp.13625>.

521 Palta, J. P. (1990). Stress interactions at the cellular and membrane levels. *HortScience*,  
522 25(11), 1377–1381.

523 Pu, Y. & Sun, D. (2015). Vis-NIR hyperspectral imaging in visualizing moisture

524 distribution of mango slices during microwave-vacuum drying. *Food Chemistry*,  
525 188, 271–278.

526 Rakesh, V., & Datta, A. (2011). Microwave puffing: Determination of optimal  
527 conditions using a coupled multiphase porous media - Large deformation model.  
528 *Journal of Food Engineering*, 107, 152–163.

529 Sagar, V. R., & Suresh, K. P. (2010). Recent advances in drying and dehydration of  
530 fruits and vegetables: a review. *Journal of Food Science and Technology*, 47(1),  
531 15–26.

532 Stępień, B. (2008). Effect of vacuum-microwave drying on selected mechanical and  
533 rheological properties of carrot. *Biosystems Engineering*, 99, 234–238.

534 Steponkus, P. L. (1984). Role of the plasma membrane in freezing injury and cold  
535 acclimation. *Ann. Rev. Plant Physiol.*, 35, 543–584.

536 The Council for Science and Technology, MEXT, Japan (2005). Analytical manual for  
537 standard tables of food composition in Japan (5th revised and enlarged ed., pp.  
538 1-40). National Printing Bureau, Tokyo. (in Japanese)

539 Therdthai, N., & Zhou, W. (2009). Characterization of microwave vacuum drying and  
540 hot air drying of mint leaves (*Mentha cordifolia* Opiz ex Fresen), *Journal of*  
541 *Food Engineering*, 91, 482–489.

542 Vaccarezza, L. M., Lombardi, J. L., & Chirife, J. (1974). Kinetics of moisture  
543 movement during air drying of sugar beet root. *International Journal of Food*  
544 *Science & Technology*, 9(3), 317–327.

545 Watanabe, T., Ando, Y., Orikasa, T., Shiina, T., & Kohyama, K. (2017). Effect of short

546 time heating on the mechanical fracture and electrical impedance properties of  
547 spinach (*Spinacia oleracea* L.). *Journal of Food Engineering*, 194, 9–14.

548 Yanyang, X., Min, Z., Mujumdar, A. S., Le-qun, Z., & Jin-cai, S. (2004). Studies on hot  
549 air and microwave vacuum drying of wild cabbage. *Drying Technology*, 22 (9),  
550 2201–2209.

551 Yongsawatdigul, J., & Gunasekaran, S. (1996). Microwave-vacuum drying of  
552 cranberries: Part I. Energy use and efficiency. *Journal of Food Processing and*  
553 *Preservation*, 20, 121–143.

554 Zhang, M. I. N., & Willison, J. H. M. (1992a). Electrical impedance analysis in plant  
555 tissues: *in vivo* detection of freezing injury. *Canadian Journal of Botany*, 70(11),  
556 2254–2258.

557 Zhang, M. I. N., & Willison, J. H. M. (1992b). Electrical impedance analysis in plant  
558 tissues: The effect of freeze thaw injury on the electrical properties of potato  
559 tuber and carrot root tissues. *Canadian Journal of Plant Science*, 72(2),  
560 545–553.

561 Zhang, M. I. N., Willison, J. H. M., Cox, M. A., & Hall, S. A. (1993). Measurement of  
562 heat injury in plant tissue by using electrical impedance analysis. *Canadian*  
563 *Journal of Botany*, 71(12), 1605–1611.

564 Zheng, X., Liu, C., Shi, J., Xue, S., Mu, Y., Lin, Z., & Liu, H. (2013). Analysis of  
565 volume expansion and dehydration rate of berry slab under microwave-vacuum  
566 puffing conditions, *LWT - Food Science and Technology*, 52, 39–48.

567 Zielinska, M., & Markowski, M. (2016). The influence of microwave-assisted drying

568 techniques on the rehydration behavior of blueberries (*Vaccinium corymbosum*  
569 L.). *Food Chemistry*, 196, 1188–1196.

570 Zielinska, M., & Michalska, A. (2016). Microwave-assisted drying of blueberry  
571 (*Vaccinium corymbosum* L.) fruits: Drying kinetics, polyphenols, anthocyanins,  
572 antioxidant capacity, colour and texture. *Food Chemistry*, 212, 671–680.

573 Zielinska, M., Ropelewska, E., & Markowski, M. (2017). Thermophysical properties of  
574 raw, hot-air and microwave-vacuum dried cranberry fruits (*Vaccinium*  
575 *macrocarpon*). *LWT - Food Science and Technology*, 85, 204–211.

576 Zielinska, M., Sadowski, P., & Błaszczak, W. (2015). Freezing/thawing and microwave-  
577 assisted drying of blueberries (*Vaccinium corymbosum* L.). *LWT - Food Science*  
578 *and Technology*, 62(1, part 2), 555–563.

579 Zielinska, M., Zielinska, D., & Markowski, M. (2018). The effect of microwave-  
580 vacuum pretreatment on the drying kinetics, color and the content of bioactive  
581 compounds in osmo-microwave-vacuum dried cranberries (*Vaccinium*  
582 *macrocarpon*). *Food and Bioprocess Technology*, 11(3), 585–602.

Figure 1

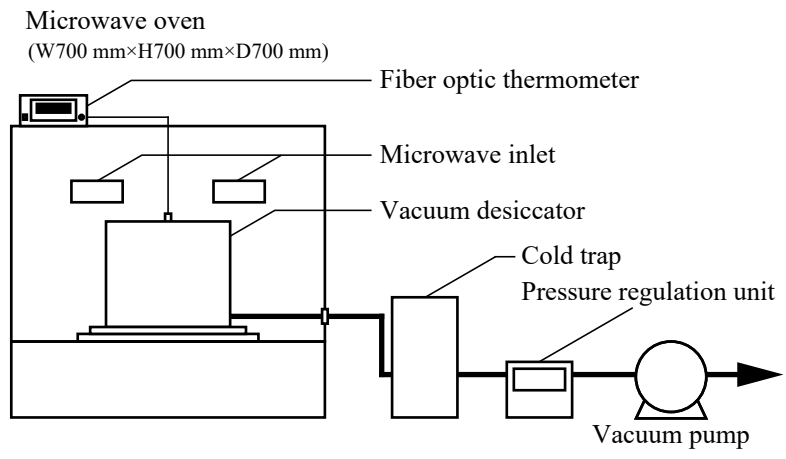


Figure 2

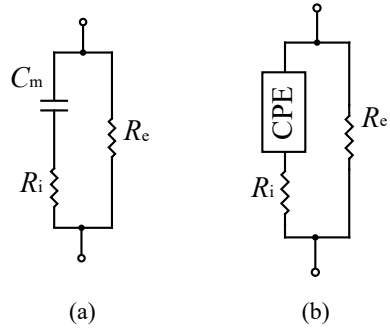


Figure 3

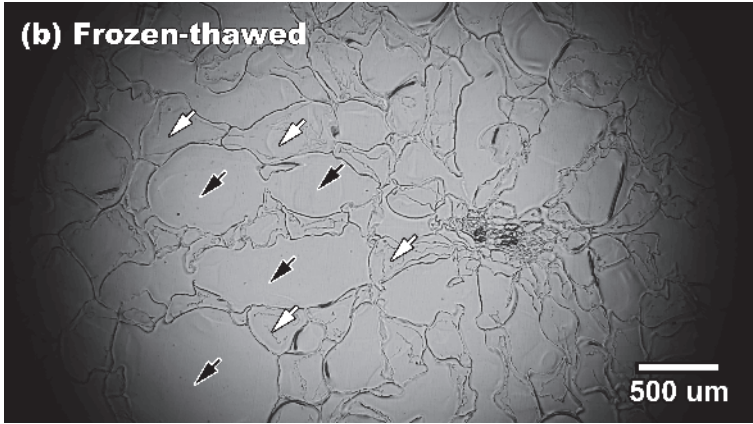
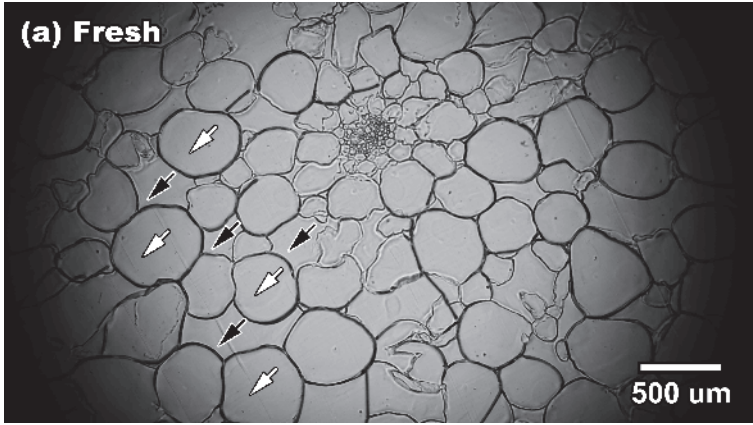
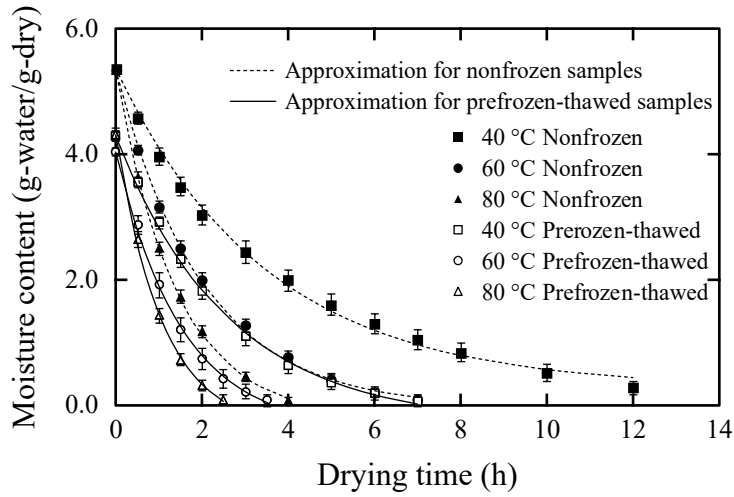


Figure 4

**(a) Air drying**



**(b) Microwave-vacuum drying**

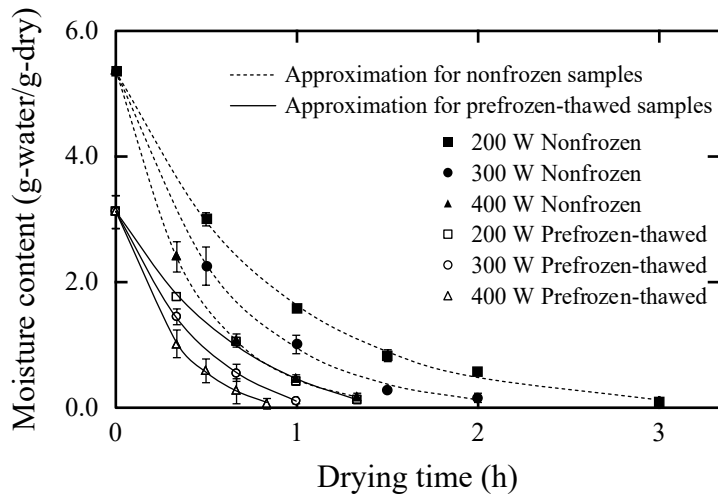
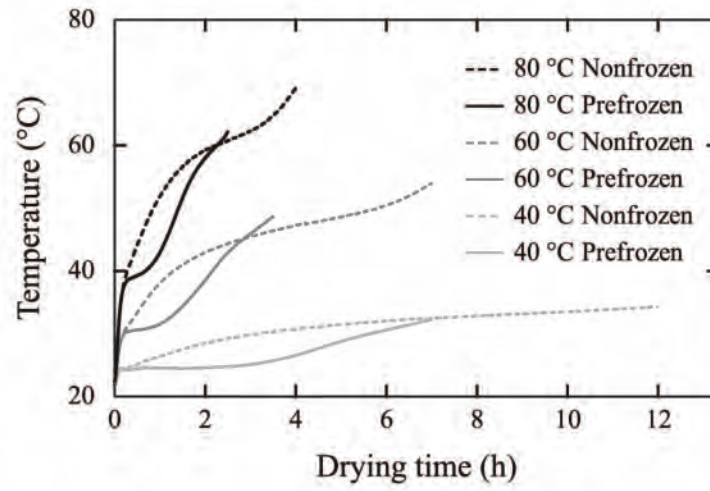




Figure 5

**(a) Air drying**



**(b) Microwave-vacuum drying**

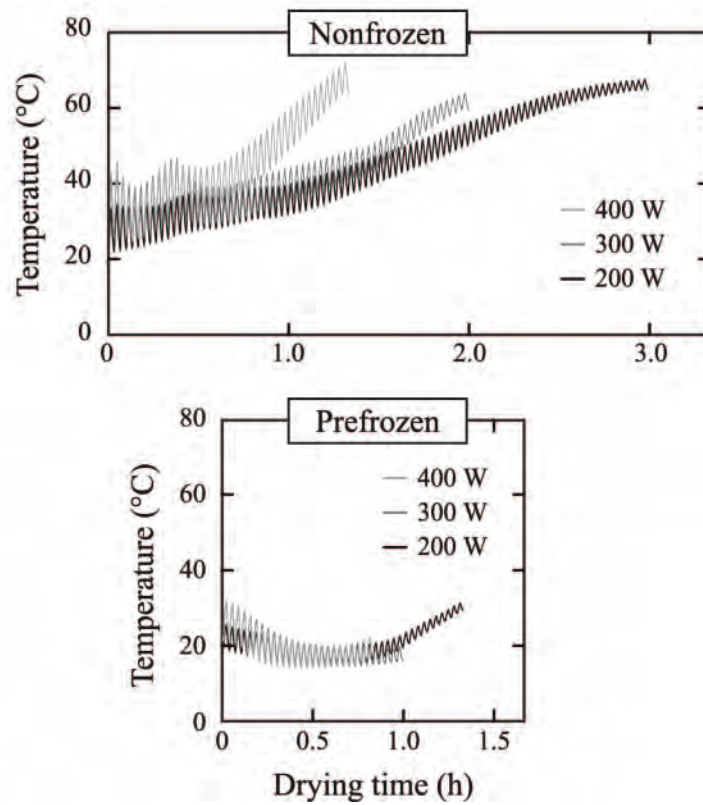
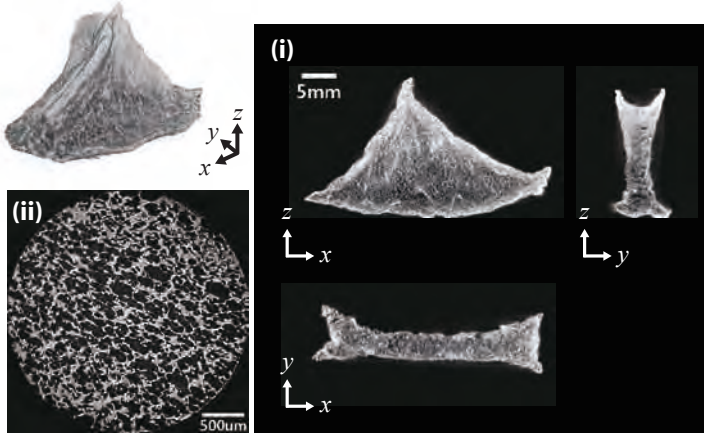
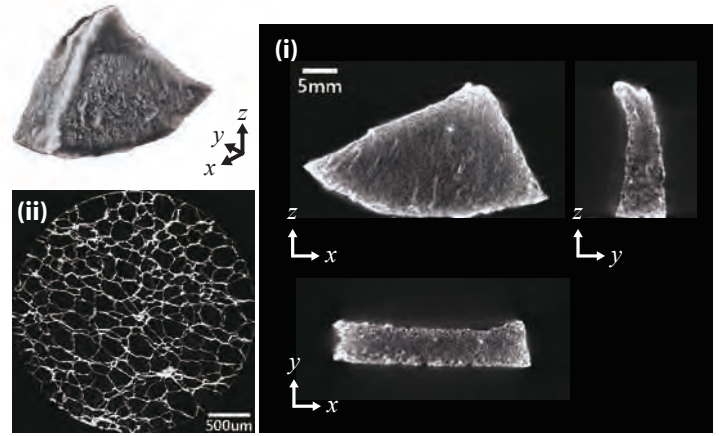


Figure 6

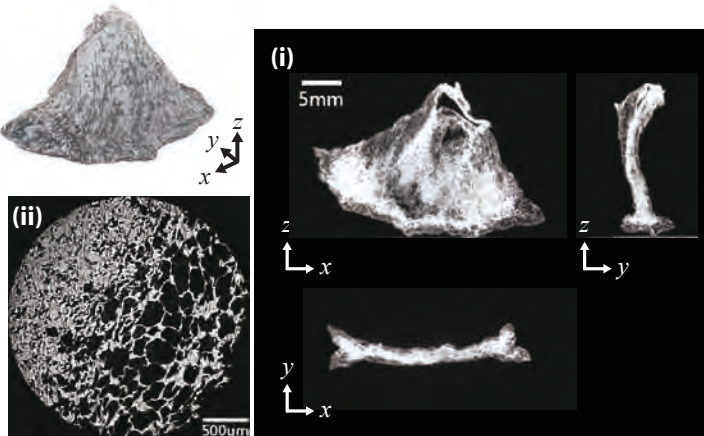
(a) AD - not treated



(b) AD - prefrozen



(c) MVD - not treated



(d) MVD - prefrozen

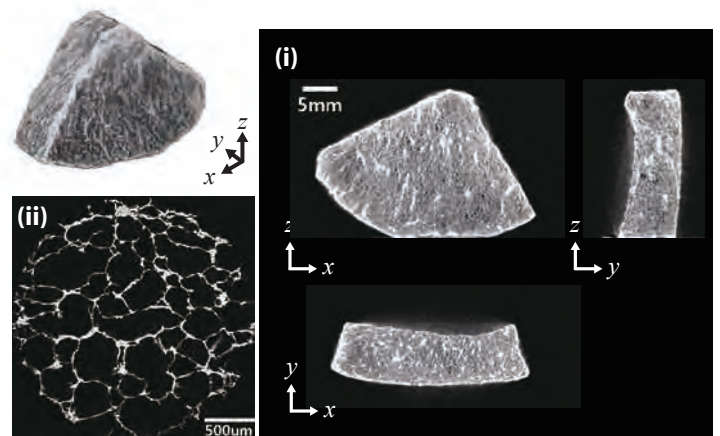


Figure 7

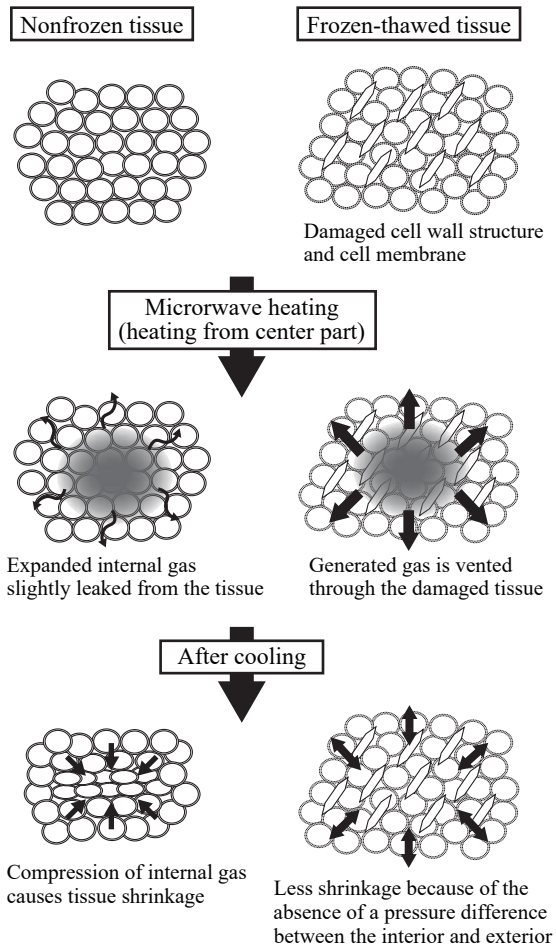
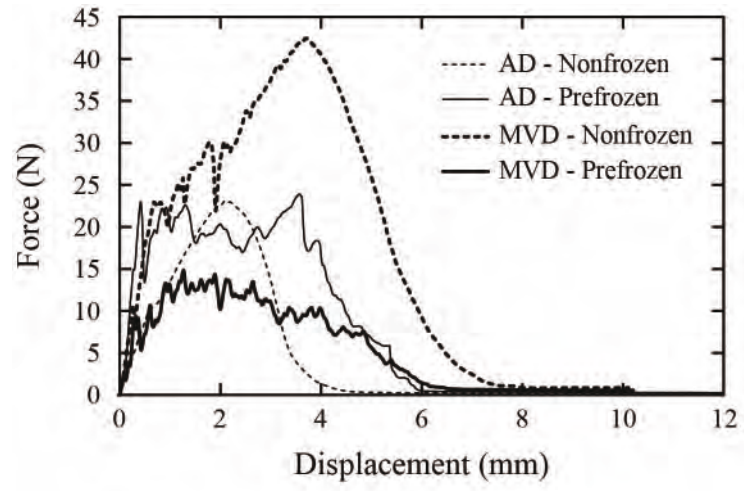


Figure 8



## Figure captions

Fig. 1. Schematic diagram of the apparatus for microwave-vacuum drying.

Fig. 2. Equivalent circuit models for biological tissues: model for single cell (a), and model for electrically inhomogeneous multiple cells with a time constant distribution (b).  $C_m$ : capacitance of cell membrane,  $R_i$ : intracellular fluid resistance,  $R_e$ : extracellular fluid resistance, CPE: constant phase element.

Fig. 3. Microscopic images of fresh (a) and frozen-thawed (b) apple flesh tissue sections. White arrows represent cells and black arrows represent intercellular spaces.

Fig. 4. Changes in the moisture content of apple samples during drying. The data are mean values of 3–4 replicates. Bars denote standard deviation. Solid and dashed lines represent the least squares regression analysis of the first-order reaction equation (Eq. 1).

Fig. 5. Changes in temperature of the central part of apple samples during drying. The data are mean values of 3–4 replicates.

Fig. 6. Reconstructed images and tomograms of the dried apple samples. AD: air dried sample at 60 °C, MVD: microwave-vacuum dried sample at a power of 300 W. (i) Whole image of the dried sample, (ii) microstructural image of the center part of the dried sample.

Fig. 7. Mechanism of the structural formation of dried apple samples during microwave-vacuum drying.

Fig. 8. Typical puncture curves of the dried apple samples. AD: air dried sample at 60 °C, MVD: microwave-vacuum dried sample at a power of 300 W.

Table 1 Equivalent circuit parameters obtained from the model fitting.

	$C_m$ (nF)	$R_e$ (k $\Omega$ )	$R_i$ (k $\Omega$ )	$R^2$
Nonfrozen	$1.64^a \pm 0.08$	$41.4^a \pm 4.5$	$3.60^a \pm 0.34$	$\geq 0.999$
Frozen-thawed	$0.41^b \pm 0.07$	$3.8^b \pm 0.6$	$6.27^b \pm 0.84$	$\geq 0.998$

$C_m$ : capacitance of cell membrane,  $R_e$ : extracellular fluid resistance,  $R_i$ : intracellular fluid resistance,  $R^2$ : determination coefficient in the model fitting. The values of  $C_m$ ,  $R_e$  and  $R_i$  represent the mean values of 16 replicates ( $\pm$  standard deviation). Different superscripts indicate significant differences ( $p < 0.01$ ) between the means in the same column compared by a  $t$ -test.

Table 2 Drying rate constant  $k$  ( $\text{h}^{-1}$ ) estimated from the exponential model for dried samples (Eq.1).

		Nonfrozen	Prefrozen
AD	40 °C	0.285	0.382
	60 °C	0.494	0.656
	80 °C	0.709	0.922
MVD	200 W	1.171	1.372
	300 W	1.674	1.945
	400 W	2.357	2.951

AD: air drying, MVD: microwave-vacuum drying.

Table 3 Mechanical parameters of the dried apple samples determined using the puncture test.

	Thickness (mm)	Maximum stress $\sigma_{\max}$ (Pa)	Elastic modulus $E$ (Pa)	Number of peaks (-)
AD - Nonfrozen	3.18 <sup>c</sup> ± 0.37	29968 <sup>b</sup> ± 3276	36886 <sup>c</sup> ± 4752	–
AD - Prefrozen	5.63 <sup>b</sup> ± 0.55	24913 <sup>bc</sup> ± 5653	260945 <sup>a</sup> ± 100959	21.27 <sup>b</sup> ± 7.23
MVD - Nonfrozen	3.25 <sup>c</sup> ± 0.44	55158 <sup>a</sup> ± 10997	140633 <sup>b</sup> ± 44150	–
MVD - Prefrozen	6.33 <sup>a</sup> ± 0.62	18941 <sup>c</sup> ± 8075	195112 <sup>ab</sup> ± 10574	42.13 <sup>a</sup> ± 7.37

AD: air dried at 60 °C, MVD: microwave-vacuum dried at 300 W. The values represent the mean values of 16–18 replicates (± standard deviation). Different superscripts indicate significant differences ( $p < 0.05$ ) between the means in the same column compared by a Tukey' s multiple range test.